JOURNAL OF SPACECRAFT AND ROCKETS
Vol. 32, No. 5, September–October 1995

On-Orbit Temperature Distribution of a Submillimeter-Telescope Primary-Reflector Panel

Glenn T. Tsuyuki* and Lloyd C. French†
Jet Propulsion Laboratory, California Institute of Technology, Pasadena, California 91109

A preliminary detailed primary-mirror thermal analysis has been performed for the Earth-orbiting Submillimeter Imager and Line Survey Telescope. The purpose of the analysis was to determine the spatial temperature distribution in a panel that composes the primary mirror. The primary mirror is formed from seven separate panels, and minimization of the temperature difference across the primary mirror is crucial to optical performance requirements. Previous work indicated that the temperature difference across the entire primary reflector mirror was small, but the nodal granularity was not sufficient to draw the same conclusion for a single panel. A finite difference model with a large number of nodes for a particular panel was developed. Automated model generator code was developed to facilitate model construction. Steady-state analyses were performed, since the transitory effects of the Earth fluxes are overwhelmed by the solar environment. The analysis indicates that the panel temperature distribution is extremely isothermal, and therefore adequate optical performance is possible. A future, more rigorous analysis now can be performed so that the figure error can be sufficiently quantified.

Introduction

THE Submillimeter Imager and Line Survey (SMILS) is a Cassegrainian telescope with a 3.65-m aperture, and it will perform a high-spectral-resolution survey of several hundreds of sources at wavelengths between 100 and 800 μm. Because of its size, the primary mirror is segmented into seven separate hexagonal panels. A large scarfed cylindrical sunshade is used to shield the primary mirror from its thermal environment. SMILS is planned to be launched on an Atlas–Centaur launch vehicle that will place it into a 24-h, 1000 by 70,000 km, 60-deg-inclination elliptical orbit. During 6 h of the orbit, near periapsis, observations are suspended, and science and engineering data are relayed to Earth stations. The SMILS payload, shown in Fig. 1, is composed of a sunshade, passively cooled Cassegrainian optics, the primary-reflector back support structure, and a superfluid-helium cryostat, which contains the science instruments. The instrument payload consists of a heterodyne radiometer, a far-infrared spectrometer, and a far-infrared camera. The required mission lifetime is 2 years.

The primary reflector is segmented into seven panels (see Fig. 2), and each panel is assumed to be a sandwich construction of aluminum or graphite–epoxy facesheets and aluminum or graphite–phenolic core. The most promising configuration is composed of graphite/epoxy facesheets and a graphite–phenolic core. The mirror surface is created by vacuum-depositing a metallized layer, and the major challenge in the panel development is to produce panels with acceptable as-manufactured surface precision without expensive refinishing. Prototype panels are now routinely being manufactured with <2-μm rms surface figures <1-μm figure change under a uniform 100-K drop from room temperature.

The figure error of the primary mirror must be at least an order of magnitude less than the observation wavelengths. The current figure error requirement for the primary mirror is 4.5 μm. Spatial temperature differences from panel to panel and within a panel must be minimized in order for this requirement to be satisfied. The spatial temperature distribution on each panel is critical in understanding the thermal distortion and hence the optical performance. It is not a straightforward task to specify acceptable temperature level and differences, since they have a complex relationship with the structural and optical design.

A thermal analysis for the SMILS telescope primary mirror was performed to determine panel-to-panel temperature differences.[1] Results indicate that the panel-to-panel temperature difference was at most 2 K, depending upon the primary reflector construction. These results were less than the 5-K strawman temperature-difference requirement, and acceptable optical performance appeared possible. The on-orbit primary-reflector panel temperatures are expected to range between 91 and 99 K. These estimates are based upon steady-state results from a system-level finite difference thermal math model of the SMILS telescope, which represents each primary reflector panel with two nodes (mirror and back side). However, there was not sufficient nodal granularity to deduce a spatial temperature distribution for an individual panel. Hence, the maximum panel-to-panel thermal difference that was predicted by the system-level thermal math model may be underestimated, since a one-node representation of the mirror side will tend to average the spatial temperature variation on the panel. To address this modeling limitation, a separate first-cut analysis was undertaken to determine the spatial temperature distribution of a single panel. This would involve nodalizing one panel from the system-level thermal math model more finely so that its temperature distribution could be ascertained. If a favorable temperature distribution within a panel is obtained, a more refined analysis could be performed.

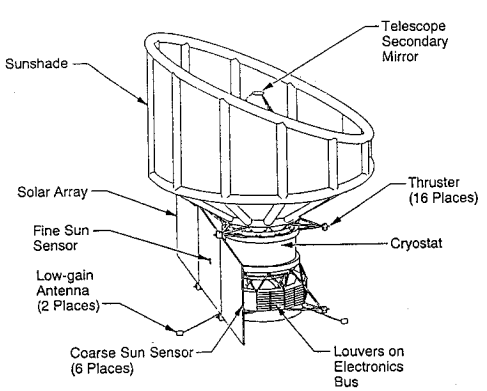

Fig. 1 SMILS telescope configuration.

Received May 3, 1994; presented as Paper 94-2006 at the AIAA/ASME 6th Joint Thermophysics and Heat Transfer Conference, Colorado Springs, CO, June 20–23, 1994; revision received April 12, 1995; accepted for publication April 28, 1995.

*Technical Group Leader, Spacecraft Thermal Engineering and Flight Operations Group, Thermal and Propulsion Engineering Section, M/S 301-358, 4800 Oak Grove Drive. Senior Member AIAA.

†Member of Technical Staff, Thermal and Fluids Systems Engineering Group, Thermal and Propulsion Engineering Section, M/S 125-129, 4800 Oak Grove Drive.

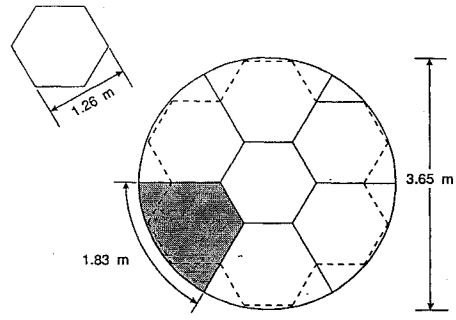

Fig. 2 Primary-reflector panel configuration.

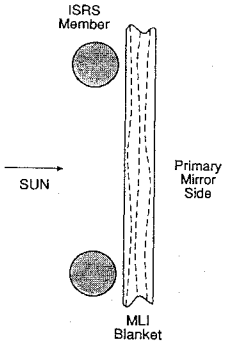

Fig. 3 Typical ISRS–MLI blanket configuration.

Approach

SMILS Telescope Thermal Design

The most visible feature of the thermal design is the inflatable sunshade (see Fig. 1). This sunshade is stowed in a container above the telescope cryostat during launch and ascent. Once in Earth orbit, the inflatable space rigidized structure (ISRS) members are inflated and cured by solar heating. Through the use of a deployment motor located in the stowage container and a pulley system on the ISRS members, multilayer insulation (MLI) blankets are then drawn between the ISRS members to complete the sunshade deployment. The blankets are drawn so that the blankets are entirely between the ISRS members and the primary mirror (see Fig. 3). Because of the capability of the blanket deployment system, the conical portion implements 15-layer MLI blankets, whereas the cylindrical portion uses 6-layer MLI blankets.

Because the telescope's own thermal background radiation can have a serious effect on the sensitivity of the science instruments (they are background-limited), it is necessary to minimize the primary reflector temperature. To this end, direct irradiation from the sun, reflected sunlight of the Earth, and thermal radiation from the Earth are not allowed to be incident upon the primary reflector. Furthermore, direct solar irradiance is not permitted on the secondary reflector or on the inside of the sunshade. However, Earth thermal emission is permitted to be incident on the sunshade interior. In order to maximize spacecraft electrical power from the solar arrays, the telescope is fixed in roll, and the pitch is restricted to no more than 25 deg off-sun pointing. Finally, yaw is only constrained by the incident-heat-flux restrictions previously indicated, and this degree of freedom is used to design science observation scenarios.

Thermal control coatings play a major role in thermally isolating the primary reflector from its environment. The portion of the sunshade exterior that is illuminated by the sun utilizes aluminized Teflon® (with the Teflon side facing outward for a low ratio of solar absorptivity to hemispherical emissivity, α_s/ϵ), which minimizes the absorbed direct solar flux. The sunshade exterior that is not illuminated utilizes aluminized Kapton® (aluminized side facing outward for low ϵ). These thermal control surfaces serve to isolate the telescope from the thermal environment. The sunshade interior utilizes the same aluminized Kapton as the nonilluminated sunshade exterior. This reduces the thermal coupling between the sunshade interior and primary reflector. The sunshade surface finishes are summarized in Fig. 4. The gap between the sunshade and the primary reflector allows the primary reflector back side to reject heat to space. The back support structure of the primary reflector structure is wrapped with 20-layer MLI blankets and the exterior layer is the same low-ϵ treatment used on the nonilluminated sunshade exterior. This serves to isothermalize the primary-reflector back side. Figure 5 graphically describes the primary-reflector thermal design.

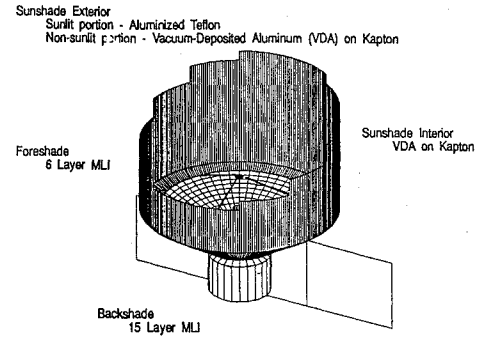

Fig. 4 System-level telescope thermal model with sunshade thermal control finishes.

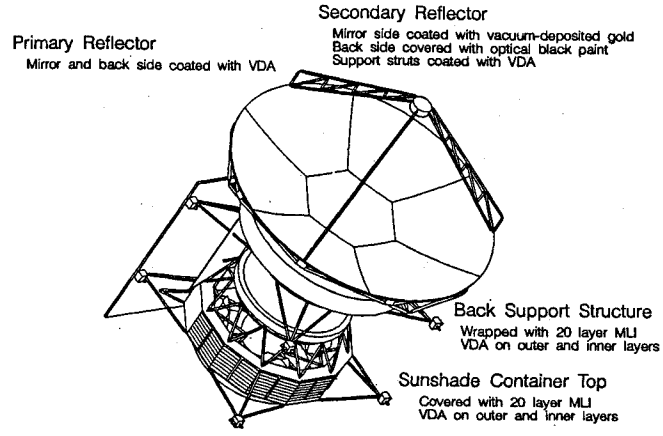

Fig. 5 Summary of primary-reflector thermal design (sunshade removed).

System-Level Telescope Thermal Math Model

The system-level thermal math model encompasses the telescope [sunshade, primary reflector, secondary reflector (with support truss), back support structure, optical bench MLI, sunshade spool MLI, and cryostat] and the spacecraft (solar panels). The finite difference model is composed of 178 nodes (see Fig. 5). Each primary reflector panel is represented by two nodes (mirror and back side). The sunshade is divided circumferentially into 12 equal divisions, and axially where the sunshade transitions from cylindrical to conical. The back support structure is not explicitly modeled, but its thermal capacitance is added to the inner layer of the back-support-structure MLI. The heat transfer through a 6- and a 15-layer blanket is modeled by extrapolating effective thermal conductivity data for 10- and 20-layer blankets, respectively.[2–4] In-plane MLI blanket heat transfer is modeled within the sunshade. For conservatism (i.e., maximizing panel temperature differences), the blankets between any pair of ISRS members are modeled as if they were thermally connected to these members. The member temperatures are driven as boundary nodes based on thermal analyses conducted by the European Space Agency.[4]

The low-ϵ surfaces were assumed to be perfectly diffuse. However, such surfaces are typically highly specular. Since the determination of radiation conductors used an extremely computationally efficient algorithms, it was decided to retain the assumption of perfectly diffuse surfaces so that timely results could be obtained. Further refined analysis using specular solution techniques will be undertaken if results are promising.

Since initial calculations demonstrated that the conductance is negligible or the hardware design implements thermal isolation by choice, all other conductive heat paths (back-support, secondary-reflector support, primary-reflector attach point to back support structure, etc.) have been neglected. Radiative edge effects between

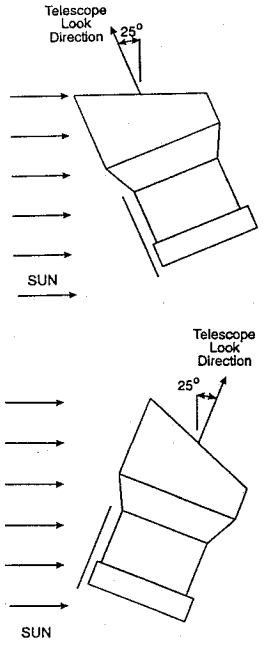

Fig. 6 Telescope orientations for cold (top) and hot (bottom) cases.

primary-reflector panels have been ignored, since panel-to-panel temperature differences have been shown to be small. From the system-level analysis, the pitch angle of the telescope had been identified as the dominant thermal parameter.[1] The thermal effect of the Earth is effectively minimized by the Earth avoidance requirements in concert with the thermal isolation provided by the sunshade and the highly elliptical orbit. In recognition of these effects, the transient on-orbit analysis can be well approximated by two bounding steady-state cases that consider only the solar environment: 1) telescope pitched 25 deg toward the sun (no Earth albedo or emissive heating); and 2) telescope pitched 25 deg away from the sun (no Earth albedo or emissive heating). These attitudes are depicted in Fig. 6. Previous analysis has demonstrated that the omission of the Earth albedo and emissive heating results in a decrease of approximately 6 K in the transient temperature history for the primary-reflector nodes, but the more critical panel-to-panel temperature difference is not significantly affected.[1] Hence omission of the Earth albedo and emissive heating does not significantly reduce the rigor of the analysis, but it greatly simplifies the analysis.

Generic Hexagonal-Panel Sub-Thermal-Math-Model Generator

Since there are a wide variety of available panel configurations, a thermal-math-model generator was developed to be able to meet the thermal analysis needs in a timely fashion. The generator is a Fortran program that may be executed on a microcomputer or VAX mainframe.[5] The generator is interactive and queries the user for number of thermal-math-model nodes, panel edge dimension, and facesheet and core thicknesses. The generator produces output (nodal capacitances and conductances) that is compatible with the thermal-math-model analyzer, Systems Improved Numerical Differencing Analyzer 1985 (SINDA85).[6] Currently, the generator creates thermal math models for flat panels, but it may be easily altered to include curvature. The nodalization methodology is currently based upon the structural-analysis finite element grid, and the general finite difference node shape is rhomboidal (an edge node is a portion of a rhombus). The nodalization of each panel layer (facesheet or core material) through the panel thickness is consistent with adjacent layers, but the number of nodes per layer may be varied (though only in the same manner for all layers). There is a thermophysical properties database (see Table 1) for many of the panel materials, and these properties are temperature-dependent according to various sources.[7,8] The generator considers different thermal conductivities for in-plane and normal-to-plane heat transfer. By using SINDA85, the panel submodel may be easily incorporated into the system-level model.

Table 1 Panel submodel generator: thermophysical property database

Material	Thermal conductivity at 25° C, W/m·K	Specific heat at 25°C, kJ/kg·K
Graphite–epoxy	3.19 (in plane) 0.91 (normal)	0.95
Al flex core	28.3 (in plane) 2.69 (normal)	0.99
Al double flex core	28.3 (in plane)	1.00
Graphite–phenolic	0.29 (in plane) 0.16 (normal)	1.04

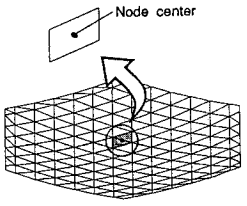

Fig. 7 Detailed panel thermal-model nodalization.

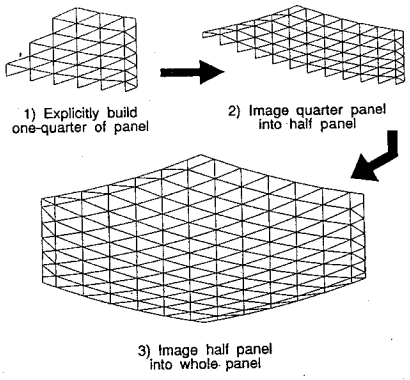

Fig. 8 Construction methodology for detailed panel geometric model.

Generic Hexagonal-Panel Sub-Geometric-Math-Model Generator

When a particular panel is finely nodalized, the determination of the radiation interchange between the detailed panel and the surrounding surfaces and of the absorbed environmental heating can be cumbersome. These radiation conductors and absorbed heating rates are used as inputs to the panel thermal math model. Once again, a geometric generator was developed in concert with the thermal-math-model generator to be able to perform a timely thermal analysis for any particular panel configuration. The geometric math model generator is also a Fortran program that may be used on the microcomputer or the VAX mainframe. The output from the geometric-math-model generator is compatible for use with the Thermal Radiation Analysis System (TRASYS),[9] which uses an optimized double-summation or Nusselt-unit-sphere scheme to determine view factors. The geometric math model is largely composed of triangular elements, since TRASYS cannot model rhomboidal surfaces explicitly. However, the corresponding triangular elements are combined within TRASYS to calculate radiation conductors and absorbed heating for the rhomboidal thermal-math-model nodes, as shown in Fig. 7. The core layer is not modeled in the geometric math model, since it is not an exterior surface. The panel shape may be spherical or parabolic. For spherical panels, the generator will ask the user to input the radius of curvature. Parabolic panels are constructed assuming the center of the panel is the vertex, and the user is asked to input the F/D ratio. An off-axis parabolic-panel option could be easily incorporated into the generator, but this capability does not currently exist. Other parameters that the user will be asked to input include the panel point-to-point or flat-to-flat dimension, number of nodal divisions along a panel edge, and mirror and backside optical properties. A local coordinate system is selected and is used to take advantage of nodalization symmetry. The powerful surface and block-coordinate-system imaging options are employed to streamline the TRASYS input file. One quarter of the panel geometry is built explicitly within a block coordinate system. The block

coordinate is imaged into itself, so that the result is half of the panel geometry. Finally, the block coordinate system is imaged into itself again to obtain the entire panel (see Fig. 8). This modeling methodology must be kept in mind when this sub-geometric-math-model is incorporated into the system-level geometric math model.

Incorporation of the Detailed Panel Submodels into the System-Level Models

Each panel has a varying view of the sunshade interior and space because of the sunshade geometry. The primary reflector panel nearest the high side of the sunshade was selected for this analysis, since this panel is expected to have the most variation in view to space as one moves from the panel edge closest to the sunshade toward the center of the primary reflector. The panel sub-geometric-math-model and sub-thermal-math-model were constructed based on the attributes that are shown in Table 2. First, the panel sub-geometric-math-model is incorporated into the system-level geometric math model (see Fig. 9). Since TRASYS did not at that time accommodate submodels readily, the chore of integrating the panel submodel to take advantage of its symmetry is cumbersome. However, there are great benefits in reduced execution time by using symmetry. TRASYS was used to calculate radiation conductors between the detailed panel nodalization and the surrounding nodes from the system-level model. For this analysis, orbital heating was not performed, since Earth albedo and planetary heating were ignored. However, the absorbed direct solar heating was computed with the system-level geometric math model without the detailed panel incorporated. Since the sunshade exterior, solar panels, and cryostat were sun-illuminated, there was no absorbed solar heating on the sunshade interior or primary reflector panels. However, if a transient orbital analysis is undertaken, orbital heating with the panel sub-geometric-math-model integrated into the system-level geometric math model must be performed.

The sub-thermal-math-model developed from the generator is much easier to incorporate into the system-level thermal math model, since SINDA85 can manage submodels. Nodal capacitances and panel conductances are incorporated in the appropriate locations within the SINDA85 input data. The radiation conductors calculated from TRASYS are also incorporated into the SINDA85 system-level telescope thermal math model.

Cases Investigated

The steady-state hot and cold cases were investigated. In either case, the Earth albedo and infrared heating were neglected. The cold case presents the minimum sunshade projected area to the sun, whereas in the hot case the projected sunshade area toward the sun is a maximum.

Table 2 Panel submodel attributes

Attribute	Value
Flat-to-flat dimension	1.26 m
Radius of curvature	2.92 m
Facesheet thickness	1.74 mm
Core thickness	25.4 mm
Nodes along panel edge	7
Total nodes	381
Mirror-side α_s/ϵ	0.14/0.03
Back-side α_s/ϵ	0.14/0.03

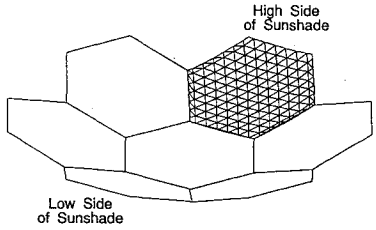

Fig. 9 Detailed panel submodel integrated into primary-reflector system-level model.

Results

Cold Case

The detailed panel was extremely isothermal. Its steady-state mirror spatial temperature distribution was essentially a constant 100 K. Temperatures were so uniform that an isotherm plot of the panel would be of no particular use. The temperature difference through the panel thickness was much less than 1 K. The maximum primary-reflector panel-to-panel temperature difference was 4 K, with panel temperatures varying from 96 to 100 K.

Hot Case

As with the cold case, the detailed panel was very isothermal, and again, no isotherm plot is given. The finely nodalized mirror panel temperature was a constant 105 K. The gradient through the thickness was larger, than in the cold case, but it was still small ($\ll$1 K). The maximum panel-to-panel temperature difference of the primary reflector was 3 K, and the panel temperatures ranged between 102 and 105 K.

Discussion of Results

The most obvious result is the constant temperature of the panel. Since the mirror side of the panel and the sunshade are both highly reflective, each panel node absorbs very little heat. Not only is the absorbed heat minimal, but it is very uniform. The thermal-math-model network was examined to determine the amount of heat flowing into each panel node from other thermal math model nodes. Since this is a steady-state analysis, the amount flowing into each panel node is equal to the amount flowing out of the same node. Since the panel node areas are not uniform, the heat flow per unit area was compiled for the panel vertex and center nodes. The fluxes are depicted in Fig. 10. For the cold case, the selected panel node heat flows vary from 319 to 347 mW/m^2, and for the hot case they varied from 369 to 404 mW/m^2. In absolute terms, the nodal thermal balance (heat flow in or out) for these particular panel nodes ranged between 0.5 and 2.0 mW for the cold case, and between 0.7 and 2.6 mW for the hot case. Although the heat flow per unit area for the center node was slightly larger than for the vertex nodes, this was offset by the radiation conductor to space being also slightly larger. Hence, the resulting panel nodal temperatures are the same.

A comparison between the system-level model without and with a detailed panel is shown in Table 3. There is good agreement between resulting panel-to-panel and through-the-thickness temperature differences. The model without the detailed panel nodalization tends to slightly underestimate the maximum panel-to-panel temperature difference (by 2 K). As expected, there are larger differences

Table 3 Comparison between system-level models without and with detailed panel nodes

Primary-reflector attribute	Without detailed panel	With detailed panel
Temperature, K	91–93 K (cold) 96–99 K (hot)	96–100 K (cold) 102–105 K (hot)
Maximum panel-to-panel temperature difference, K	2 (cold) 3 (hot)	4 (cold) 3 (hot)
Through-the-thickness temperature difference, K	$\ll$1 (cold) <1 (hot)	$\ll$1 (cold) <1 (hot)

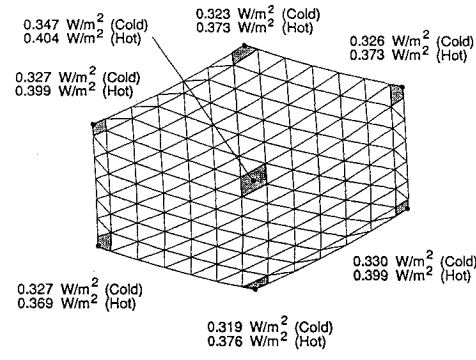

Fig. 10 Total heat flow per unit area into vertex and center panel nodes.

associated with the absolute temperature level of the primary reflector, as much as 7 K. For the purposes of quantifying optical performance, the primary-reflector temperature differences (i.e., panel to panel and within a single panel) are much more important than the absolute temperature of the primary reflector. If one assumes that the most accurate temperatures are obtained with an infinite number of nodes in the thermal model, the error for the temperature difference within a single panel can be bounded by the difference in the maximum panel-to-panel temperature difference between the models with and without the detailed panel nodalization. The cold case demonstrates that the bounding error for the temperature difference within a panel is 2 K. With a 2-K variation across a single panel, the maximum panel-to-panel temperature difference would be 6 K, and this could result in marginal primary-reflector figure error.

This preliminary analysis indicates that the spatial panel temperature variations are virtually absent, which implies that the resulting figure error from thermal distortions will be small. However, when the accuracy of this analysis is considered, the panel temperature variation could be as large as 2 K, which may result in marginal figure error. Further structural and optical analyses are required to judge the acceptability of the 2-K panel temperature variation. If the results of these analyses are positive, the panel thermal analysis must be revisited, since it has been predicated on one crucial assumption, i.e., that the highly reflective surfaces are diffuse. In actuality, the highly reflective surfaces are more likely to be specular. However, this preliminary analysis provided timely results for a multidisciplinary design process. Rather than undertaking a time-consuming approach (i.e., radiation conductor determination via ray tracing), a quick and approximate approach was implemented so that the design space could be narrowed in a timely manner. In the near future, a more rigorous analysis may be performed using specular solution techniques.

Acknowledgments

The work described in this paper was conducted by the Jet Propulsion Laboratory, California Institute of Technology, under a contract with NASA. The authors would like to express their appreciation to Richard Helms and Chris Porter from the Jet Propulsion Laboratory for their useful technical comments and discussions throughout the duration of this work.

References

[1]Tsuyuki, G., and Cohen, E., "Thermal Design Optimization of a Segmented GFRP Primary Reflector for a Submillimeter Telescope," *Design of Optical Instruments*, edited by D. M. Aikens, V. L. Genberg, G. C. Krumweide, and M. J. Thomas, Proceedings of the Society of Photo-Optical Instrumentation Engineers, Vol. 1690, Bellingham, WA, March 1992, pp. 265–272.

[2]DeVault, G., Russell, D., and Rose, C., "Orbiter Midsection/Payload Thermal Math Model Description," NASA Johnson Space Center, Rept. ES3-76-1, Rev. D, June 1983.

[3]Stroom, C., "Spacecraft Thermal Control Design Data, ESA (TST-02)," Vol. 2, European Space Agency, Noordwijk, The Netherlands, 1984, Sec. J, pp 3-1–3-157.

[4]Anon., "FIRST Inflatable Thermal Shield, Phase 1—Final Report," Contraves, European Space Agency Contract Rept. 6324/85/NL/PB(SC), Noordwijk, The Netherlands, June 1987.

[5]French, L., "User's Memo for Hexagonal Panel Thermal Math Model Generator," private communication, Jet Propulsion Lab., Pasadena, CA, Aug. 1991.

[6]Cullimore, B. A., Goble, R. G., Jensen, C. L., and Ring, S. G., "SINDA '85/FLUINT, Systems Improved Numerical Differencing Analyzer and Fluid Integrator, Version 2.2," COSMIC–Univ. of Georgia, Rept. MSC-21528, Athens, GA, Nov. 1987.

[7]Porter, C. C., "LDR/PSR Materials List," personal communication, Jet Propulsion Lab., Pasadena, CA, April 1990.

[8]Anon., "Thermal Properties of Gr/E PBD Materials," Rockwell International, Rept. IL-75-993-1357, Downey, CA, Feb. 5, 1975.

[9]Anderson, G. E., and Garcia, D., "Thermal Radiation Analyzer System (TRASYS) User's Manual," COSMIC–Univ. of Georgia, Rept. MSC-21959, Athens, GA, April 1988.

I. E. Vas
Associate Editor